Ilam University of Medical Sciences

Journal of Basic Research in Medical Sciences

Online ISSN: 2383-0972
Print ISSN: 2383-0506

Homepage: https://jbrms.medilam.ac.ir

Comparison of singular value decomposition and Fourier deconvolution methods for cerebral blood flow quantification in dynamic contrast-enhanced magnetic resonance imaging

Seyed Salman Zakariaee[1]✉, Hasan Hashemi[2], Hossein Salmanipour[2]

[1] Department of Medical Physics, Faculty of Paramedical Sciences, Ilam University of Medical Sciences, Ilam, Iran
[2] Department of Radiology, Faculty of Medicine, Ilam University of Medical Sciences, Ilam, Iran

Article Info

Article type:
Research Article

Article history:
Received: 30 Nov. 2020
Revised: 21 Feb. 2021
Accepted: 14 Dec. 2021
Published online: 9 Jun. 2023

✉**Correspondence to:**
Seyed Salman Zakariaee, Department of Medical Physics, Faculty of Paramedical Sciences, Ilam University of Medical Sciences, Ilam, Iran.
Tel: +98 9188783551
Fax: +98 8432227122
Email: salman_zakariaee@yahoo.com

ABSTRACT

Introduction: Glioma grading is an important clinical procedure that determines the procedure of the patient's treatment. There is an increasing interest in other complementary techniques in addition to histo-pathological evaluation as the gold standard method. Perfusion indices have shown promising correlations with histo-pathological grades and neovascularization degrees in gliomas. In this study, the processing times and classification performances of cerebral blood flow (CBF) parameters calculated using singular value decomposition (SVD) and Fourier deconvolution methods were evaluated.

Materials and Methods: The statistical differences between the CBF magnitudes of the high- and low-grade gliomas were evaluated for eighteen patients with pathologically proven gliomas (Low-grade gliomas, 5; High-grade gliomas, 13). The classification performances of the calculated indices were evaluated using the receiver operating curve analysis.

Results: The deconvolution processing times for the SVD method were significantly higher than those of the Fourier deconvolution method (about ~9 times). There were statistically significant differences in both CBF indices between the high- and low-grade gliomas ($P<0.05$). In ROC curve analysis, CBF indices calculated by the SVD method had a higher area under the curve (about 8538.5 vs. 8153.8).

Conclusion: Based on the study, the glioma grade might be determined using the Fourier-based CBF index with an almost similar grading efficiency and a much lower processing time than the CBF index calculated by the SVD method.

Keywords: Glioma grading, Dynamic contrast-enhanced MRI, Cerebral blood flow, Singular value decomposition, Fourier deconvolution

How to cite this article: Zakariaee SS, Hashemi H, Salmanipour H. Comparison of singular value decomposition and Fourier deconvolution methods for cerebral blood flow quantification in dynamic contrast-enhanced magnetic resonance imaging. J Bas Res Med Sci. 2022; 9(4) :57-68.

Publisher: Ilam University of Medical Sciences

Introduction

Gliomas are the most common primary cerebral neoplasms which are classified as hyper-vascularized malignant tumors. Angiogenesis plays an essential role in tumor growth, invasion, and metastasis(1-4). The glioma grading is an important clinical procedure that determines the procedure of the patient's treatment. The histopathological assessment is considered the gold standard method for glioma grading. Inherent sampling errors of the biopsy procedure result in tumor misclassifications (5-7). Hence, there is an increasing interest in other complementary techniques such as imaging approaches. The magnetic resonance imaging (MRI) method is the most frequently non-invasive imaging modality that is used to evaluate brain tumors. Conventional MRI techniques have the inherent limitations to evaluate the proliferation potential of the tumor (8, 9). Recently, a number of the more sophisticated MRI techniques have been introduced which allow assessing the physiological parameters in the brain tissues (8, 10).

Perfusion weighted-magnetic resonance imaging (PW-MRI) method is one of the clinically most relevant procedures of functional MRI which is used to assess microvasculatures, tumor neovascularization, and capillary permeability. The assessment of tumor hemodynamics (including blood flow, blood volume, and vessel permeability) would give considerable insight into the angiogenic process of the tumor (3, 11). Perfusion indices have shown promising correlations with histological grades and degrees of neovascularization in gliomas which provide the possibility of tumor grading and therapeutic follow-up of brain tumors(10, 11). Dynamic susceptibility contrast (DSC) and arterial spin-labeling (ASL) MRI techniques are the most widely used procedures to evaluate the brain perfusion indices. Cerebral blood volume (CBV), cerebral blood flow (CBF), and mean transit time (MTT) are conventional perfusion indices that can be quantified in these methods. DSC-MRI technique could quantify the perfusion indices with a better signal-to-noise ratio and lower imaging time. Therefore, it's a preferred method over the ASL method (8, 12, 13). DSC-MRI has been used for glioma grading and differentiation between the tumor types by many authors (14-16). These perfusion indices could be also calculated based on dynamic contrast-enhanced MRI (DCE-MRI) data (17, 18). Therefore, both the perfusion and permeability indices could be extracted using a single dose dynamic imaging, simultaneously. In the DCE-MRI method, tissue concentration is described by the convolution of the concentration-time curve in the arteries (Ca(t)) with the residue curve (R(t)) (18, 19). In pioneer studies, different deconvolution methods including SVD and Fourier deconvolution have been used for CBF quantification (3, 18). In this study, the processing times and the classification performances of CBF parameters calculated using Fourier and SVD deconvolution methods were evaluated.

Methods and Materials

Imaging Protocols

All images were acquired using a 3-Tesla clinical MRI scanner (TrioTim, Siemens Medical Solutions, Erlangen, Germany) and an 8-channel coil head. The pre-and post-contrast T1-weighted spin-echo imaging was performed with the following parameters: TR/TE= 690/18 msec; flip angle= 55°; slice thickness= 5 mm; number of averages=1; intersection gap=1 mm; matrix= 256 × 192. Other pre-contrast anatomical images were obtained using transverse FLAIR (TR/TE, 3111/6 msec; TI, 1238; flip angle, 90°; echo train length, 7; slice thickness, 5 mm; number of averages, 0.5; intersection gap, 1 mm; matrix, 512 × 512) and transverse T2-weighted spin-echo (TR/TE, 3300/93; echo train length, 11; flip angle, 120°; slice

thickness, 5 mm; number of averages, 2; intersection gap, 1 mm; matrix, 384 × 288) sequences.

The parameters of the gradient recalled echo sequence (GR) for dynamic contrast-enhanced T1- weighted imaging were TR=3.8 msec, TE=1.34 msec, field of view=200 × 200 mm^2, matrix size =233 × 256, flip angle=15°, NEX=1, slice thickness=5 mm, and gap= 1 mm. At the end of the sixth acquisition, Gd-DTPA (0.1 mL/kg) was injected intravenously at a rate of 2 mL/second, followed immediately by a bolus injection of 15 ml saline flush at the same rate.

Patients

In this study, eighteen patients (male-female ratio, 6:12; mean age, 46.44 years; age range, 21-78 years) were evaluated and their glioma grades were determined using the surgical pathology diagnosis as the gold standard method(5 patients with low-grade gliomas and 13 patients with high-grade gliomas). The study was approved by the local committee for medical research ethics. Informed consent was obtained from all of the patients prior to the study. The tumor ROI was determined by referencing the FLAIR and post-contrast T1-weighted images for the low- and high-grade glioma patients, respectively. The mean value of CBF within the tumor ROI was considered.

CBF Quantification Based on the DCE-MRI Method

Cerebral blood flow index (CBF) could be derived based on DCE-MRI data as an alternative dynamic imaging method. Tissue concentration (C (t)) in the form of Ca (t) ⊗R (t) is determined using the equation 1:

$$C(t)= \rho \, . \, H \, . \, CBF. \, (C_a(t) \otimes R(t)) \qquad (1)$$

Where ⊗ is the convolution operator and R(t) is the residual function. CBF is described as the part of arterial blood volume that is delivered to the brain tissue per time (in mL/100gr.min).

In this study, Fourier and SVD deconvolution methods are used for CBF calculation(18, 19). Equation 1 could be simplified using the Fourier transform deconvolution method as:

$$CBF.R = \frac{1}{\rho \, .H} \, F^{-1} \left\{ \frac{F\{C(t)\}}{F\{ Ca(t)\}} \right\} \qquad (2)$$

Where F-1{} denotes the inverse Fourier transformation. CBF would be determined using the inverse Fourier transformation of $\frac{F\{C(t)\}}{F\{ Ca(t)\}}$ at every time point with known arterial input and time-contrast concentration curve.

In the SVD convolution method, the singular value decomposition of the real or complex matrix M is described as the equation 3:

$$M = U \sum V^* \qquad (3)$$

Where U is an m×m real or complex unitary matrix, $\sum$ is an m×n rectangular diagonal matrix with non-negative real numbers on the diagonal, and V is an n×n real or complex unitary matrix. The diagonal elements (λ_i) of $\sum$ are the singular values of M. The matrix of M is reduced to a bidiagonal matrix using Householder reflections with a cost of $4mn^2 - 4n^3/3$ flops. It was assumed that only singular values are needed. The SVD of the bidiagonal matrix is solved using the QR algorithm for the computation of eigenvalues.

Statistical Analysis

The statistical differences between the CBF magnitudes of the high- and low-grade gliomas were evaluated using the independent student T-test analysis. For CBF magnitudes calculated using Fourier and SVD deconvolution methods, the classification performances of these indices were evaluated using the receiver operating

curve (ROC) analysis. The accuracy, sensitivity, specificity, positive predictive (PPred), and negative predictive (NPred) values of the different CBF thresholds were determined according to pathology results as the gold standard method.

In this study, the agreement between the grading approaches (including the pathology results and both CBF indices) was determined using the Kappa index. The magnitude of the kappa index is ranged from zero to 1. A better agreement between the two grading methods is achieved when the Kappa coefficient is closer to 1. Kappa coefficient is described using equation 4.

$$k = \frac{p(a) - p(e)}{1 - p(e)} \quad (4)$$

Where P(a) and P(e) are respectively the observed and expected agreements between the glioma grades determined using both grading approaches. P(a) and P(e) were determined using the following equations.

$$P(a) = \frac{TH+TL}{TH+TL+FH+FL} \quad (5)$$

$$P(e) = \frac{TH+FL}{TH+TL+FH+FL}\frac{TH+FH}{TH+TL+FH+FL}\frac{TL+FH}{TH+TL+FH+FL}\frac{TL+FL}{TH+TL+FH+FL} \quad (6)$$

Where TH is the number of patients that were correctly classified as high-grade gliomas, TL is the number of patients that were correctly classified as low-grade gliomas, FH is the number of patients that were wrongly classified as high-grade gliomas, and FL is the number of patients that were wrongly classified as low-grade gliomas. The p-value was set to 0.05 as the statistical significance level in each analysis.

Results

For each patient, CBF maps were achieved using both Fourier and SVD deconvolution methods. The extracted CBF maps for the patients with different glioma grades are shown in Figures 1-4. The transverse T2-Weighted, Flair, pre- and post-contrast T1-Weighted images were also depicted in these figures.

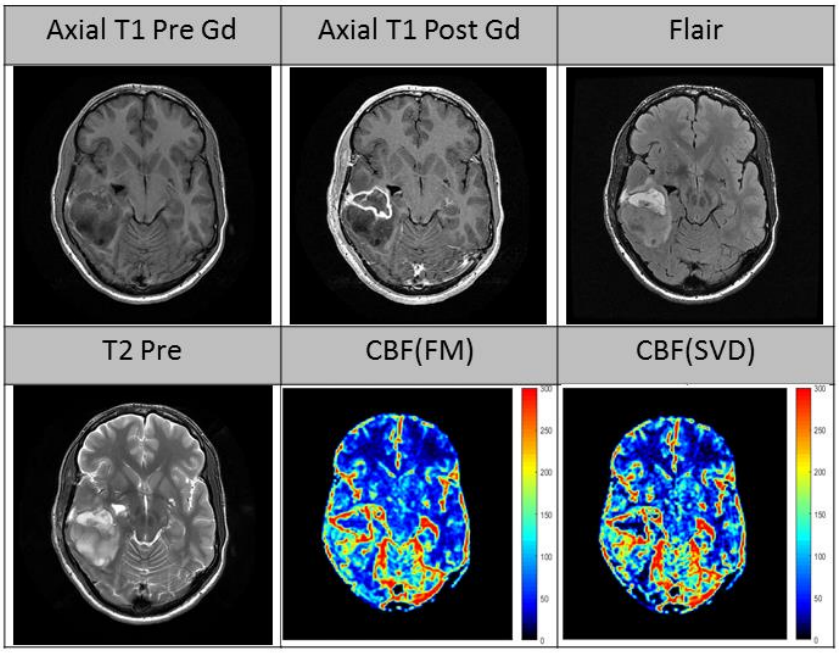

Figure 1. The extracted MRI images for a 25-year-old man with right temporal high-grade oligoastrocytoma. (a) Axial pre-contrast T1-weighted image. (b) Axial post-contrast T1-weighted image. This image shows an enhanced lesion in the right temporal lobe. (c) Axial T1-weighted FLAIR image. There is an ill-defined mass with higher signal intensity than the normal brain tissue. (d) Axial T2-weighted image. This image shows an ill-defined mass with high signal intensity. (e,f) The extracted CBF maps using Fourier and SVD deconvolution methods, respectively. These maps show low CBF values within the tumor, which is similar to the normal brain tissue. There is a well-discriminated border with high CBF values around the tumor.

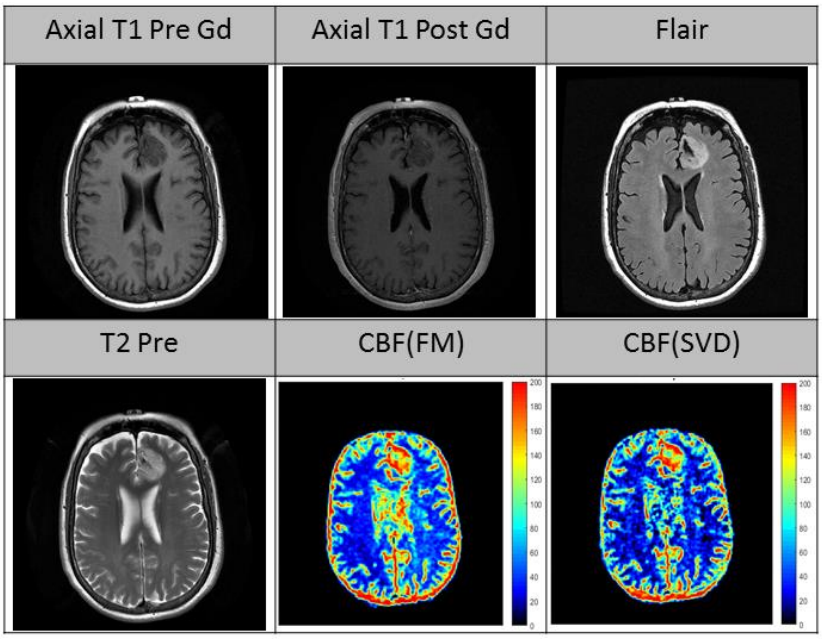

Figure 2. The extracted MRI images for a 62-year-old woman with left frontal low-grade oligodendroglioma. (a) Axial pre-contrast T1-weighted image. (b) Axial postcontrast T1-weighted image. This image shows an enhanced lesion in the left medial-frontal lobe and anterior cingulate gyrus. (c) Axial T1-weighted FLAIR image. There is an ill-defined mass with higher signal intensity than the normal brain tissue. (d) Axial T2-weighted image. This image shows an ill-defined mass with high signal intensity. (e,f) The extracted CBF maps using Fourier and SVD deconvolution methods, respectively. These maps show high CBF values for the tumor than the normal brain tissue.

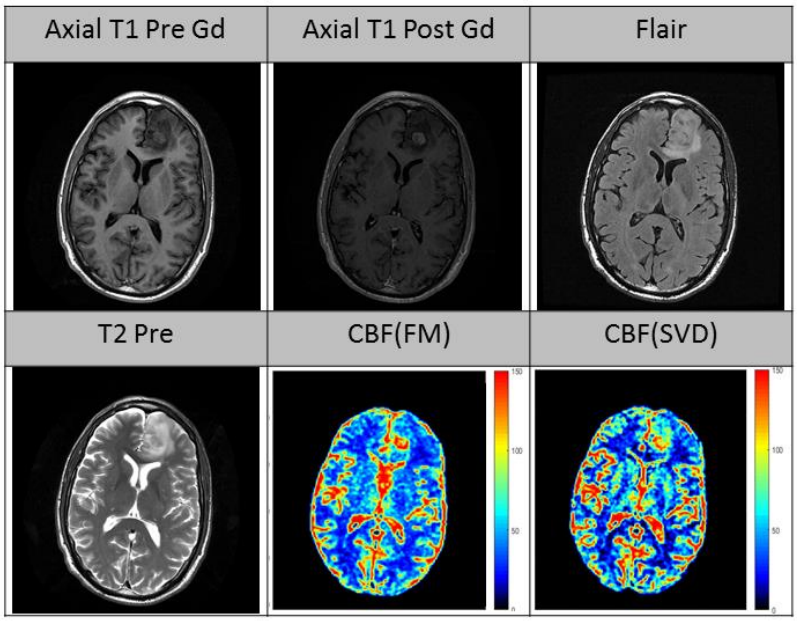

Figure 3. The extracted MRI images for a 48-year-old man with left frontal low-grade oligodendroglioma. (a) Axial pre-contrast T1-weighted image. (b) Axial postcontrast T1-weighted image. This image shows an enhanced lesion in the left medial-frontal lobe and anterior cingulate gyrus. (c) Axial T1-weighted FLAIR image. There is an ill-defined mass with higher signal intensity than the normal brain tissue. (d) Axial T2-weighted image. This image shows an ill-defined mass with high signal intensity. (e,f) The extracted CBF maps using Fourier and SVD deconvolution methods, respectively. These maps show high CBF values for the tumor than the normal brain tissue.

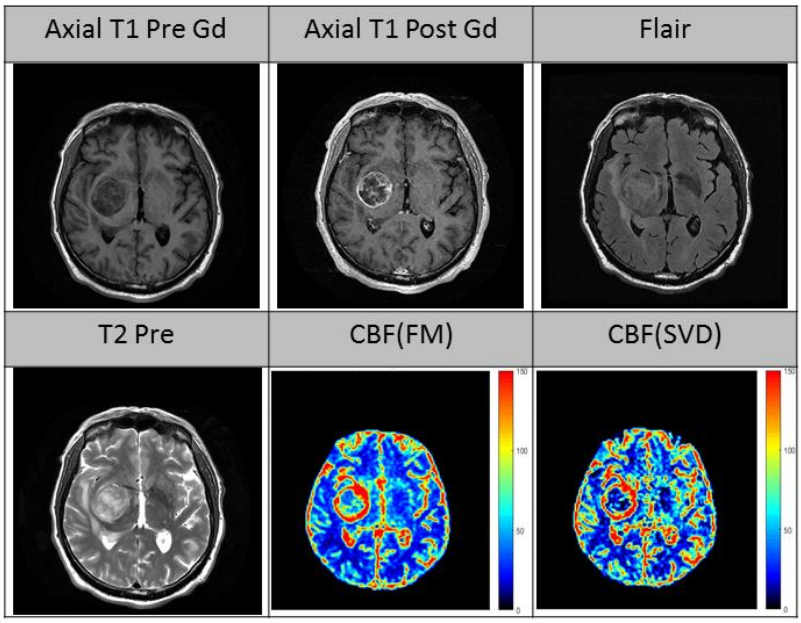

Figure 4. The extracted MRI images for a 67-year-old man with right insular GBM. (a) Axial pre-contrast T1-weighted image. (b) Axial postcontrast T1-weighted image. This image shows an enhanced lesion involved with the right insular lobe and basal ganglia. (c) Axial T1-weighted FLAIR image. There is an ill-defined mass with higher signal intensity than the normal brain tissue. (d) Axial T2-weighted image. This image shows an ill-defined mass with high signal intensity. (e,f) The extracted CBF maps using Fourier and SVD deconvolution methods, respectively. These maps show low CBF values within the tumor, which is similar to the normal brain tissue. There is a well-discriminated border with high CBF values around the tumor.

The Descriptive Statistics of the Processing Times for Fourier and SVD Deconvolution Methods

In the CBF quantification for each patient, the processing times of Fourier and SVD deconvolution methods were recorded. The descriptive statistics of these processing times are listed in Table 1. Box-and-whisker plots of the processing times were also depicted in Figure 5.

Table 1. The descriptive statistics of the processing times for the Fourier and SVD deconvolution methods in CBF quantifications.

Studied Parameter	N	Mean ± SD
FT - CBF (mL/100gr.min)	18	0.45 ± 0.75E-2
SVD - CBF (mL/100gr.min)	18	3.93 ± 0.24E-1

FT – CBF and SVD – CBF were respectively noted instead of the processing times for the Fourier and SVD deconvolution methods.

The Statistical Differences of Calculated CBF Indices between the High- and Low-grade Gliomas

The statistical differences of calculated CBF indices between the high- and low-grade gliomas were evaluated using the independent samples T-Test statistical analysis. The descriptive statistics of the CBF indices for the high- and low-grade gliomas are listed in Table 2. For both CBF indices calculated using Fourier and SVD deconvolution methods, the P-values are listed in the last column.

The Optimal Discriminative Thresholds of CBF Indices Calculated using Fourier and SVD Deconvolution Methods to Differentiate the High- and Low-grade Gliomas

The best thresholds of the calculated CBF parameters to discriminate the high- and low-grade gliomas were determined using the receiver operating characteristic (ROC)

analysis. For CBF indices calculated using the Fourier and SVD deconvolution methods, different discriminative thresholds were selected and their accuracy, sensitivity, specificity, Kappa coefficient, positive predictive (PPred), and negative predictive (NPred) values were evaluated according to the pathological results as the gold standard method. The ROC curve was plotted based on these magnitudes. The ROC curves of CBF indices calculated using Fourier and SVD deconvolution methods are plotted in Figure 6.

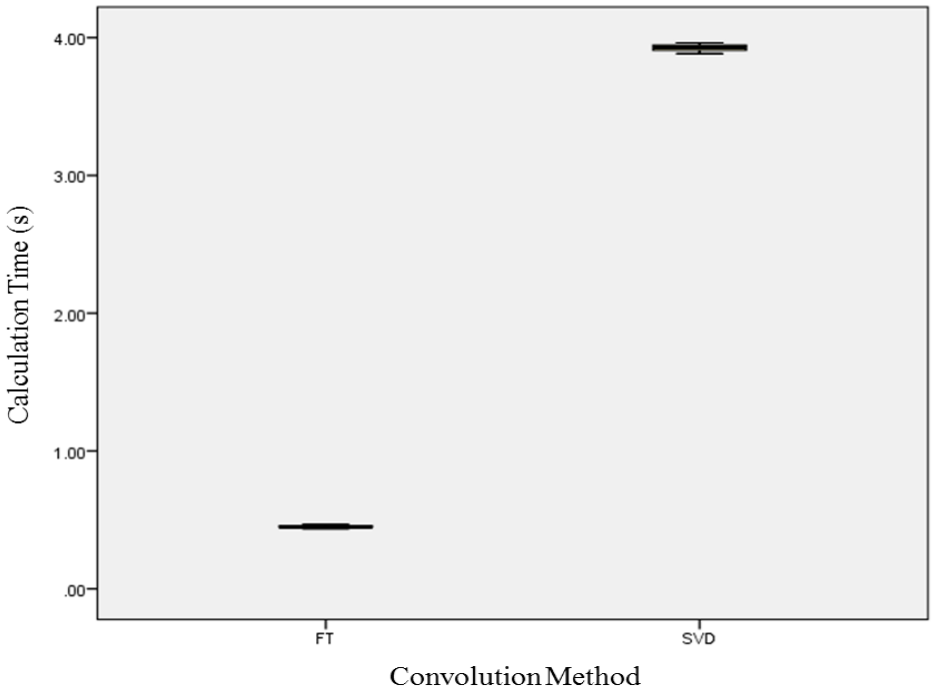

Figure 5. Box-and-whisker plots of the processing times for Fourier and SVD deconvolution methods in CBF quantification. The middle line is the median value. The inferior and superior extremes of the box correspond to the first and third quartiles, respectively. FT and SVD were respectively noted instead of the processing times for Fourier and SVD deconvolution methods.

Table 2. The descriptive statistics of CBF magnitudes calculated using Fourier and SVD deconvolution methods for the high- and low-grade gliomas. For each studied parameter, the P-value is listed in the last column.

Studied parameter	Grade	N	Mean ± SD	P value
FT – CBF (mL/100gr.min)	Low-Grade	5	163.41 ± 76.52	
	High-Grade	13	247.79 ± 70.87	0.04
SVD – CBF (mL/100gr.min)	Low-Grade	5	160.98 ± 57.88	
	High-Grade	13	244.01 ± 76.49	0.04

FT – CBF and SVD – CBF were respectively noted instead of CBF magnitudes calculated using Fourier and SVD deconvolution methods.

The optimal discriminative thresholds of CBF indices calculated using the Fourier and SVD deconvolution methods to discriminate the high- and low-grade gliomas are listed in Table 3. The accuracy, sensitivity, specificity, Kappa coefficient, positive predictive, and negative predictive values for the optimal thresholds were also listed in Table 3.

The overall grading performances of the CBF parameters could be determined using the area under the ROC curve (AUC). The area under the ROC curves (AUCs) of CBF indices calculated using Fourier and SVD deconvolution methods are listed in Table 4.

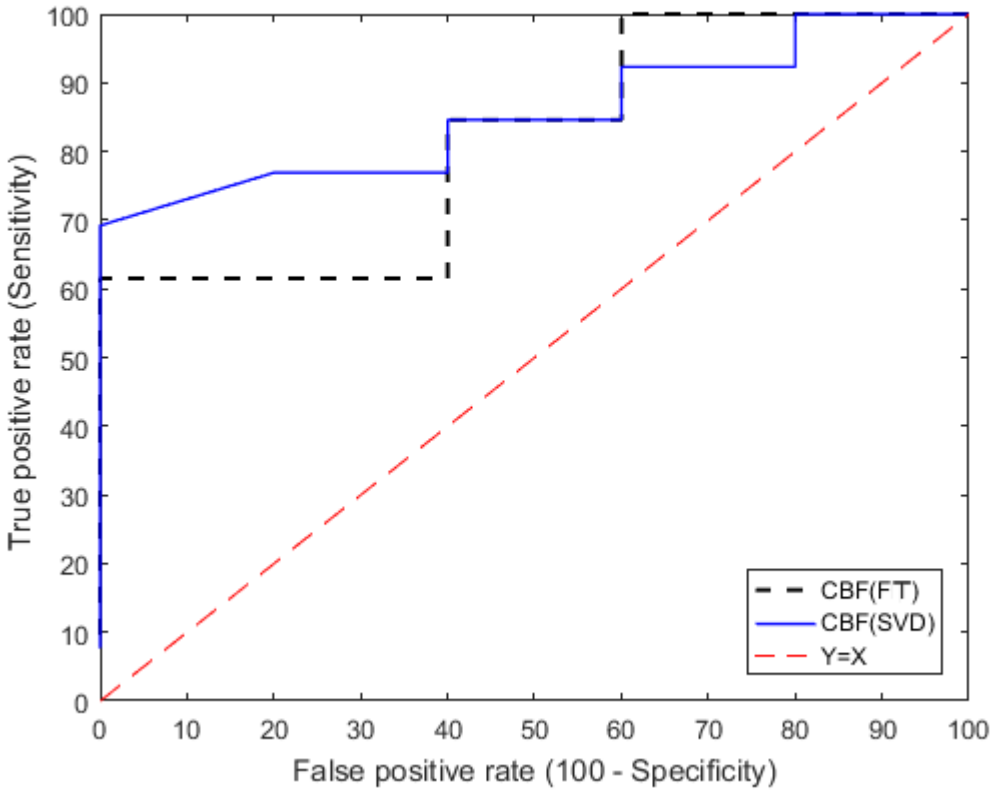

Figure 6. Receiver operating characteristic curves of CBF indices calculated using Fourier and SVD deconvolution methods to differentiate the high- and low-grade gliomas. The "Y=X" curve was also depicted in the graph. CBF (FT) and CBF (SVD) were respectively noted instead of CBF magnitudes calculated using Fourier and SVD deconvolution methods.

Table 3. The optimal discriminative thresholds of CBF indices calculated using Fourier and SVD deconvolution methods to differentiate the high- and low-grade gliomas. The accuracy, sensitivity, specificity, Kappa coefficient, positive predictive, and negative predictive values for the optimal thresholds were also listed.

Parameter	Threshold	Accuracy	Sensitivity	Specificity	Positive predictive value	Negative predictive value	Kappa coefficient
FT – CBF (mL/100gr.min)	169.64-179.82	77.78	84.62	60.00	84.62	60.00	0.77
SVD – CBF (mL/100gr.min)	181.07-203.70	77.78	84.62	60.00	84.62	60.00	0.77

FT - CBF and SVD - CBF were respectively noted instead of CBF magnitudes calculated using Fourier and SVD deconvolution methods.

Table 4. AUCs of CBF indices calculated using Fourier and SVD deconvolution methods.

Parameter	AUC
FT – CBF (mL/100gr.min)	8153.8
SVD – CBF (mL/100gr.min)	8538.5

FT - CBF and SVD - CBF were respectively noted instead of CBF magnitudes calculated using Fourier and SVD deconvolution methods.

Discussion

The histopathological assessment as the gold standard method for glioma grading has inherent limitations that result in tumor misclassifications (5-7). Hence, there is an increasing interest in other complementary techniques such as imaging approaches. Perfusion indices (including CBV and CBF) have shown promising correlations with histopathological grades and neovascularization degrees in gliomas(10,

11). Therefore, they could be a good complementary technique for histopathological assessment. These perfusion indices are conventionally quantified using the DSC- and ASL-MRI methods. Perfusion indices could be also extracted using a single dose DCE-MR imaging(17, 18). In the DCE-MRI method, different deconvolution methods including Fourier and SVD deconvolution approaches have been used for CBF quantification (3, 18). In this study, the processing times and classification performances of DCE-CBF parameters calculated using Fourier and SVD deconvolution methods were evaluated.

The processing times of Fourier and SVD deconvolution methods for CBF quantification were depicted in graph 1. As could be seen from the graph, the processing times for the SVD deconvolution method are significantly higher than those of the Fourier deconvolution method. The SVD method is almost 9 times more time-consuming than the Fourier deconvolution approach.

The statistical differences of calculated CBF indices between the high- and low-grade gliomas were evaluated. The descriptive statistics of the CBF indices for the high- and low-grade gliomas and the results of the observed differences in their means between the two groups are listed in Table 2. There were statistically significant differences for both CBF indices between the high- and low-grade gliomas. Therefore, the high- and low-grade gliomas could be accurately discriminated by these parameters.

Cellularity and vascularity of the tumor are two of the main factors which are considered for the histopathological classification of gliomas. For high-grade gliomas, the enhanced areas with higher CBF magnitudes are more expected than those of the low-grade gliomas (20, 21). For both deconvolution methods, higher CBF magnitudes were quantified for the high-grade gliomas. Studies have shown that this parameter could be used as a bioimaging marker for glioma grading with a high true-positive and low false-negative rates (22-24). In Pauliah et al study, an improved T1-weighted dynamic contrast-enhanced MRI method was used to probe the microvascularity and heterogeneity of human gliomas. Twenty–five patients with brain tumors underwent the DCE-MR examinations and rCBV and rCBF indices were calculated based on these T1-Weighted DCE-MRI data. In their study, rCBF values for high- and low-grade gliomas were 3.94±1.47 and 2.25±0.87, respectively. There was a significant difference in the rCBF index between the high- and low-grade gliomas (3). Their results were in line with our findings.

The optimal discriminative thresholds of CBF indices calculated using the Fourier and SVD deconvolution methods to discriminate the high- and low-grade gliomas were listed in Table 3. The accuracy, sensitivity, specificity, Kappa coefficient, positive predictive, and negative predictive values for these optimal thresholds were also listed in this table. The best discriminative thresholds for CBF indices calculated using Fourier and SVD deconvolution methods were 169.64-179.82 mL/100gr.min and 181.07-203.70 mL/100gr.min, respectively. These results indicated that the CBF indices calculated using Fourier and SVD deconvolution methods have similar grading efficacies.

In ROC curve analysis, the CBF index calculated using the SVD deconvolution method has a higher AUC (about 8538.5 vs. 8153.8). For the ideal grading system with classification efficacy equal to 100%, The maximum magnitude of the area under the curve is 10000. Therefore, the CBF index calculated using the SVD deconvolution method has a better performance for glioma grading.

In this study, the processing times of the deconvolution procedures for Fourier and SVD methods and the grading performances of CBF indices calculated using these deconvolution methods were evaluated. The results showed that the

Fourier deconvolution method has a much lower processing time despite the similar grading efficacy. The acceptable correlations between the tumor grades and the CBF indices were achieved for both calculated CBF indices.

In the evaluated approach, the perfusion and permeability parameters (including Ktrans, Kep, etc.) could be extracted using single-dose DCE-MR imaging. Therefore, a more complete collection of physiological indices would be obtained using a single-dose acquisition. T1-Weighted DCE-MRI is hardly affected by susceptibility artifacts and provides higher spatial resolution while maintaining imaging times in the acceptable range(25).

Conclusion

In this study, the processing times and the glioma grading efficacies of CBF indices calculated using Fourier and SVD deconvolution methods were evaluated. Based on the results, it could be concluded that the glioma grades could be determined using the Fourier - based CBF index with an almost similar classification efficacy and a much lower processing time than the CBF index quantified by the SVD deconvolution method.

Conflict of Interest

The authors declare that they are no conflicts of interest .

References

1. Jia Z, Geng D, Xie T, Zhang J, Liu Y. Quantitative analysis of neovascular permeability in glioma by dynamic contrast-enhanced MR imaging. J Clin Neurosci. 2012;19(6):820-3. doi: 10.1016/j.jocn.2011.08.030.
2. Tate MC, Aghi MK. Biology of angiogenesis and invasion in glioma. Neurother. 2009;6(3):447-57. doi: 10.1016/j.nurt.2009.04.001.
3. Pauliah M, Saxena V, Haris M, Husain N, Rathore RKS, Gupta RK. Improved T 1-weighted dynamic contrast-enhanced MRI to probe microvascularity and heterogeneity of human glioma. Magn Reson Imaging. 2007;25(9):1292-9. doi: 10.1016/j.mri.2007.03.027.
4. Li X, Zhu Y, Kang H, Zhang Y, Liang H, Wang S, et al. Glioma grading by microvascular permeability parameters derived from dynamic contrast-enhanced MRI and intratumoral susceptibility signal on susceptibility weighted imaging. Cancer Imaging. 2015;15(4):1-9. doi: 10.1186/s40644-015-0039-z.
5. Awasthi R, Rathore RK, Soni P, Sahoo P, Awasthi A, Husain N, et al. Discriminant analysis to classify glioma grading using dynamic contrast-enhanced MRI and immunohistochemical markers. Neuroradiology. 2012;54(3):205-13. doi: 10.1007/s00234-011-0874-y.
6. Daumas-Duport C, Scheithauer B, O'Fallon J, Kelly P. Grading of astrocytomas: a simple and reproducible method. Cancer. 1988;62(10):2152-65. doi: 10.1002/1097-0142(19881115)62:10<2152::aid-cncr2820621015>3.0.co;2-t.
7. Hakyemez B, Erdogan C, Ercan I, Ergin N, Uysal S, Atahan S. High-grade and low-grade gliomas: differentiation by using perfusion MR imaging. Clin Radiol. 2005;60(4):493-502. doi: 10.1016/j.crad.2004.09.009.
8. Cebeci H, Aydin O, Ozturk-Isik E, Gumus C, Inecikli F, Bekar A, et al. Assesment of perfusion in glial tumors with arterial spin labeling; comparison with dynamic susceptibility contrast method. Eur J Radiol. 2014;83(10):1914-9. doi: 10.1016/j.ejrad.2014.07.002.
9. Al-Okaili RN, Krejza J, Wang S, Woo JH, Melhem ER. Advanced MR Imaging Techniques in the Diagnosis of

Intraaxial Brain Tumors in Adults 1. Radiographics. 2006;26(suppl_1):173-89. doi:10.1148/rg.26si065513.

10. Jiang J, Zhao L, Zhang Y, Zhang S, Yao Y, Qin Y, et al. Comparative analysis of arterial spin labeling and dynamic susceptibility contrast perfusion imaging for quantitative perfusion measurements of brain tumors. Int J Clin Exp Pathol. 2014;7(6):2790-9.
11. Gagner JP, Law M, Fischer I, Newcomb EW, Zagzag D. Angiogenesis in gliomas: imaging and experimental therapeutics. Brain Pathol. 2005;15(4):342-63. doi: 10.1111/j.1750-3639.2005.tb00119.x.
12. Ye J, Bhagat SK, Li H, Luo X, Wang B, Liu L, et al. Differentiation between recurrent gliomas and radiation necrosis using arterial spin labeling perfusion imaging. Exp Ther Med. 2016;11(6):2432-6. doi: 10.3892/etm.2016.3225.
13. Rau MK, Braun C, Skardelly M, Schittenhelm J, Paulsen F, Bender B, et al. Prognostic value of blood flow estimated by arterial spin labeling and dynamic susceptibility contrast-enhanced MR imaging in high-grade gliomas. J Neurooncol. 2014;120(3):557-66. doi: 10.1007/s11060-014-1586-z.
14. Yang D, Korogi Y, Sugahara T, Kitajima M, Shigematsu Y, Liang L, et al. Cerebral gliomas: prospective comparison of multivoxel 2D chemical-shift imaging proton MR spectroscopy, echoplanar perfusion and diffusion-weighted MRI. Neuroradiology. 2002;44(8):656-66. doi: 10.1007/s00234-002-0816-9.
15. Shin JH, Lee HK, Kwun BD, Kim J-S, Kang W, Choi CG, et al. Using relative cerebral blood flow and volume to evaluate the histopathologic grade of cerebral gliomas: preliminary results. AJR Am J Roentgenol. 2002;179(3):783-9. doi: 10.2214/ajr.179.3.1790783.
16. Hartmann M, Heiland S, Harting I, Tronnier VM, Sommer C, Ludwig R, et al. Distinguishing of primary cerebral lymphoma from high-grade glioma with perfusion-weighted magnetic resonance imaging. Neurosci Lett. 2003;338(2):119-22. doi: 10.1016/s0304-3940(02)01367-8.
17. Sourbron S, Ingrisch M, Siefert A, Reiser M, Herrmann K. Quantification of cerebral blood flow, cerebral blood volume, and blood–brain-barrier leakage with DCE-MRI. Magn Reson Med. 2009;62(1):205-17. doi: 10.1002/mrm.22005.
18. Singh A, Haris M, Rathore D, Purwar A, Sarma M, Bayu G, et al. Quantification of physiological and hemodynamic indices using T1 dynamic contrast-enhanced MRI in intracranial mass lesions. J Magn Reson Imaging. 2007;26(4):871-80. doi: 10.1002/jmri.21080.
19. Østergaard L, Weisskoff RM, Chesler DA, Gyldensted C, Rosen BR. High resolution measurement of cerebral blood flow using intravascular tracer bolus passages. Part I: Mathematical approach and statistical analysis. Magn Reson Med. 1996;36(5):715-25. doi: 10.1002/mrm.1910360510.
20. Calli C, Kitis O, Yunten N, Yurtseven T, Islekel S, Akalin T. Perfusion and diffusion MR imaging in enhancing malignant cerebral tumors. Eur J Radiol. 2006;58(3):394-403. doi: 10.1016/j.ejrad.2005.12.032.
21. Rizzo L, Crasto SG, Moruno PG, Cassoni P, Ruda R, Boccaletti R, et al. Role of diffusion-and perfusion-weighted MR imaging for brain tumour characterisation. Radiol Med. 2009;114(4):645-59. doi: 10.1007/s11547-009-0401-y.
22. Bangiyev L, Espagnet MCR, Young R, Shepherd T, Knopp E, Friedman K, et al., editors. Adult brain tumor imaging: state of the art. Semin Roentgenol; 2014: Elsevier. doi: 10.1053/j.ro.2013.11.001.

23. Keunen O, Taxt T, Grüner R, Lund-Johansen M, Tonn J-C, Pavlin T, et al. Multimodal imaging of gliomas in the context of evolving cellular and molecular therapies. Adv Drug Deliv Rev. 2014;76:98-115. doi: 10.1016/j.addr.2014.07.010.
24. Arvinda H, Kesavadas C, Sarma P, Thomas B, Radhakrishnan V, Gupta A, et al. Glioma grading: sensitivity, specificity, positive and negative predictive values of diffusion and perfusion imaging. J Neurooncol. 2009;94(1):87-96. doi: 10.1007/s11060-009-9807-6.
25. Zakariaee SS, Oghabian MA, Firouznia K, Sharifi G, Arbabi F, Samiei F. Assessment of the agreement between cerebral hemodynamic indices quantified using dynamic susceptibility contrast and dynamic contrast-enhanced perfusion magnetic resonance imagings. J Clin Imaging Sci. 2018;8(2):1-9. doi:10.4103/jcis.JCIS_74_17. eCollection 2018.